

Dielectrics Newsletter

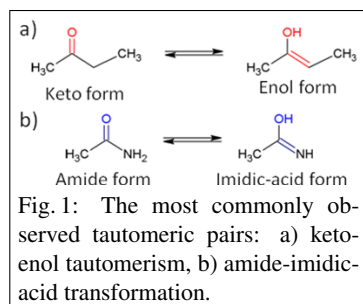
Scientific newsletter for dielectric and impedance spectroscopy

Issue July 2011

Z. Wojnarowska, P. Włodarczyk,
M. Paluch

Broadband Dielectric Spectroscopy – a New Tool for the Investigation of Tautomerization and Mutarotation Phenomena in Organic Compounds

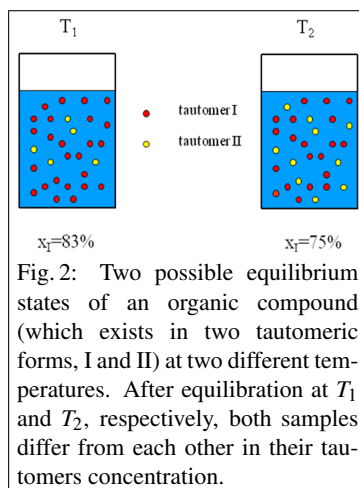
This paper will show how to employ broadband dielectric spectroscopy (BDS) to investigate the tautomerization and mutarotation phenomena in organic compounds. According to the commonly accepted definition, tautomerization is observed when one isomer of organic compound converts itself into another form (tautomer) [1]. Tautomerization usually involves the movement of a hydrogen atom between different locations on the molecule, resulting in two or more different molecular structures. The most commonly observed examples of this phenomenon are reversible transformations between ketone - enol forms and amide-imidic acid forms (see Fig. 1).



The tautomerization phenomenon is of great importance especially in medicinal chemistry and biochemistry because different isomers may play various roles in living organisms. That is why understanding of this process has long been a subject of experimental study and theoretical considerations.

There is a number of experimental data which show that tautomerism occurs mainly in solutions, in gas phase, or in the amorphous material. In the liquid state, there are

usually two or more tautomer forms for a given material. However, the exact ratio of the isomers depends on several factors, including temperature, solvent, and pH. Herein, using the BDS technique we focus only on the temperature effect on the tautomers equilibrium observed in two states, i.e., the supercooled liquid and the glassy material. As schematically shown in Fig. 2, at a given temperature, two different tautomers exist in dynamic equilibrium with each other. However, when temperature is changed, the system's re-equilibration begins, i.e., the tautomers concentration ratio is changing. It is interesting to note that the chemical equilibration process at this new temperature may take much longer than the time required for the thermal stabilization of the sample at this temperature, in some cases even a few days.



The main goal of this paper is to demonstrate how easily one can monitor the chemical equilibration process using dielectric spectroscopy. It is well known that tautomers of a given chemical compound often very often show differences in their chemical and physical properties, such as dipole moment, the molecular relaxation time or glass transition temperature. Since all these properties can be determined from dielectric measurements, the BDS technique can be effectively used for monitoring the

kinetics of the tautomerization phenomenon. If tautomers differ from each other in the glass transition temperature T_g , the sample equilibration at constant temperature leads to a fluctuation of viscosity. As a consequence, the α -relaxation time (τ_α), observed in the dielectric spectrum, will vary with time during the chemical equilibration process. The same behavior is expected in the case of dc conductivity. On the other hand, the changes of the average dipole moment value of the quenched sample observed during tautomerization are correlated with the variation of static permittivity (ϵ_s). Moreover, from the behavior of the static permittivity of sample and the dipole moment of both tautomers, it should be possible to predict the direction of tautomerization [2].

To describe the kinetics of the tautomerization, i.e., to calculate the activation energy and recognize the real time scale of this process at various temperature conditions, several isothermal time dependent dielectric measurements are required. In our previous work we have shown that with decreasing temperature, the equilibration slows down and might even take a couple of days to complete [3]. Since the dielectric measurements are completely automated, even a tautomerization process lasting several days can easily be monitored.

In this paper, we present studies on the tautomerization phenomenon of glibenclamide and the mutarotation process of monosaccharides – anhydrous D-ribose and anhydrous D-fructose as examples. Glibenclamide (GCM) is one of the pharmaceuticals used to treat type II of diabetes mellitus. The experiments done so far show that there are two centers in the GCM molecule at which tautomerization may occur. While the first one tautomeric center is characteristic only for the GCM molecule, the second one is the backbone of the whole group of sulfonylurea drugs. The proton transfer observed in GCM

molecule is commonly known as the amide-imidic acid tautomerism [4]. At the melting temperature, the tautomerization process is very fast (the amide form observed in the crystalline sample begin transformation into the imidic-acid form). However, after quenching one can observe the sample re-equilibration connected with the decreasing amount of the less energetically stable imidic-acid tautomers. The vitrification of the freshly prepared glass occurs at 327 K. If the sample is then equilibrated above T_g for a few days, the isomeric ratio changes due to the tautomerization process. This new equilibrium with higher population of amide forms also has a higher glass transition temperature (338 K) [5].

In the case of monosaccharides, the tautomerization process, usually called mutarotation, is more complicated. In general, monosugars can be found in four different cyclic forms: two six-membered (α and β pyranoses) and two five-membered rings (α and β furanoses). It is important to note that mutarotation can be regarded as a process of transformation from one tautomer to another with the open ring (chain) stage. In the crystalline state, both anhydrous fructose and anhydrous ribose occur only in β -pyranose form. During the melting process, mutarotation is induced and β -pyranoses begin transformation into the furanose forms. However, in the vitrified state, D-ribose as well as D-fructose tautomers are

in an equilibrium which lies predominantly to the pyranose side, thus dielectric spectroscopy monitor furanose to pyranose transformations [6].

To investigate the tautomerism phenomenon of supercooled GCM drug and the mutarotation process of monosaccharides, we have performed time dependent dielectric measurements at a few different temperatures. In Fig. 3, the dielectric spectra of glibenclamide (panel a) and D-ribose (panel b) evolving in time at 365 K and 299 K, respectively, are depicted. As one can see, in both cases relaxation time is getting longer in time (structural relaxation curve is shifting towards lower frequencies) while an opposite behavior is found for the dc conductivity.

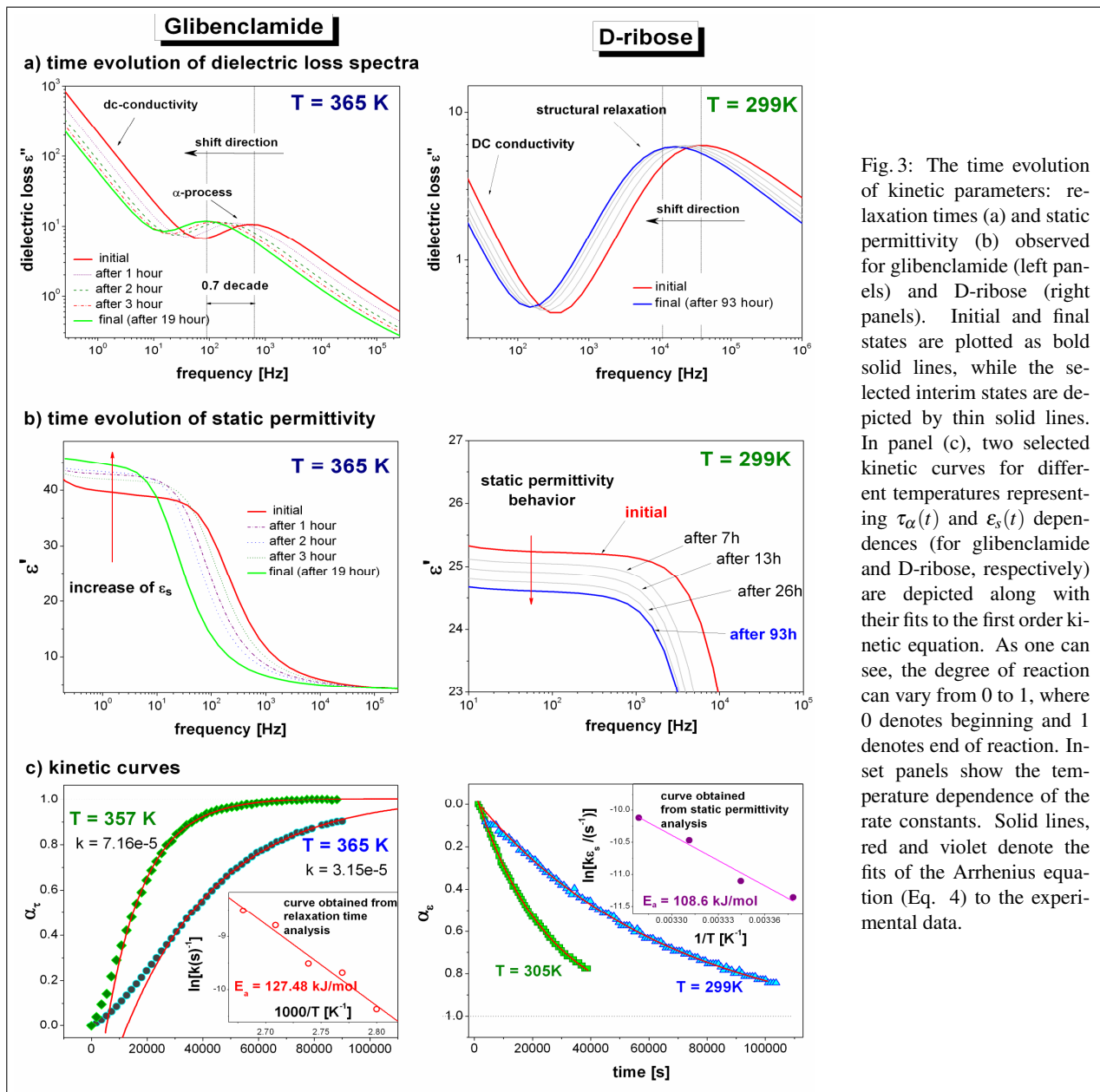


Fig. 3: The time evolution of kinetic parameters: relaxation times (a) and static permittivity (b) observed for glibenclamide (left panels) and D-ribose (right panels). Initial and final states are plotted as bold solid lines, while the selected interim states are depicted by thin solid lines. In panel (c), two selected kinetic curves for different temperatures representing $\tau_\alpha(t)$ and $\epsilon_s(t)$ dependences (for glibenclamide and D-ribose, respectively) are depicted along with their fits to the first order kinetic equation. As one can see, the degree of reaction can vary from 0 to 1, where 0 denotes beginning and 1 denotes end of reaction. Inset panels show the temperature dependence of the rate constants. Solid lines, red and violet denote the fits of the Arrhenius equation (Eq. 4) to the experimental data.

Simultaneously, both samples exhibit different static permittivity behavior – while in the case of glibenclamide, ϵ_s slightly increases, a decreasing trend is observed for D-ribose. One can find that the change of relaxation time, dc conductivity as well as static permittivity corresponds to the rate of tautomerism. Thus, to establish the rate of the tautomerization process at different temperature conditions, analysis of the evolution in time of only one of the mentioned parameters is sufficient. Description of mutarotation kinetics of D-ribose was performed by monitoring changes of static permittivity in time while in the case of glibenclamide the analysis of relaxation times was chosen to examine the tautomerization kinetics. For comparison of the kinetic curves ($\tau_\alpha(t)$ and $\epsilon_s(t)$) obtained at different temperatures in one graph, the degree of reaction (α), rather than values of α relaxation times and static permittivity, has to be used. It has been achieved by using normalized value of τ_α vs. time or ϵ_s vs. time:

$$\alpha = \frac{p - p_0}{p_f - p_0} \quad (1)$$

For every temperature, p_0 is the first measured value of τ_α or ϵ_s ((10 ± 3) min after melting) while p_f corresponds to τ_α or ϵ_s measured in the final equilibrium state. The representative kinetics curves, constructed by plotting these parameters versus time, are presented in the lower panels of Fig. 3. As one can see, the kinetic curves obtained for gliben-

clamide and D-ribose show exponential character, i.e., the product concentration is raised to the first power. The experimental data can thus be satisfactorily described by first-order kinetics:

$$\alpha = 1 - A \cdot \exp(-kt) \quad (2)$$

where α is the degree of reaction (concentration equivalent); t time; A preexponential factor, and k is the rate of reaction – one of the most important parameter which describes kinetics. With use of the rate constant, k we can calculate the half-time of the examined process:

$$\tau_{1/2} = \frac{\ln 2}{k} \quad (3)$$

Moreover, using the values of k determined at different temperature conditions, we are able to calculate the activation energy of the tautomeric conversion. As shown in the inset panels of Fig. 3, the logarithm of the rate constant is linearly related to $1/T$. Thus, from the fit of Arrhenius equation (Eq. 4) to the experimental data the activation energy barrier of tautomerization and mutarotation processes can be easily determined.

$$\ln k = \ln A - \frac{E_a}{RT} \quad (4)$$

It is well known that the knowledge of the kinetic parameters is one of the keys to determine the reaction mechanisms in solid phases. In the case of drugs which reveal tautomerism, measurements of the parameters k and $t_{1/2}$ are needed for the determination of its accurate treatment conditions. It follows from the fact that

change in temperature means different tautomer equilibrium and consequently different bioavailability of amorphous drug. In the case of GCM, the value of k determined experimentally above the glass transition conditions can be also used to estimate the half-life time at room temperature. At 298 K, it is equal to almost three years. This means that one can expect the amide and imidic acid form to co-exist in amorphous GCM for more than five years. Since the literature reports that this kind of equilibrium detected in the glassy state strongly reduces the tendency of drug crystallization, one can expect that the amorphous sample may be stored for five years without any sign of crystallization [5].

We have already presented how tautomerization phenomenon affects the structural relaxation, and how the kinetics of this process can be observed. However, α relaxation is not the only one process sensitive to isomerization. In some cases, freshly quenched and equilibrated samples may differ from each other in secondary relaxations. This kind of phenomenon can be observed, e.g., in the case of monosaccharides (D-ribose and D-fructose). Since the furanose ring is more flexible and has more internal degrees of freedom than the pyranose one, the change of the γ relaxation character is expected during mutarotation. To study this possible effect, we have performed two measurements of this process, before and after sample equilibration, both at the same temperature in the glassy state.

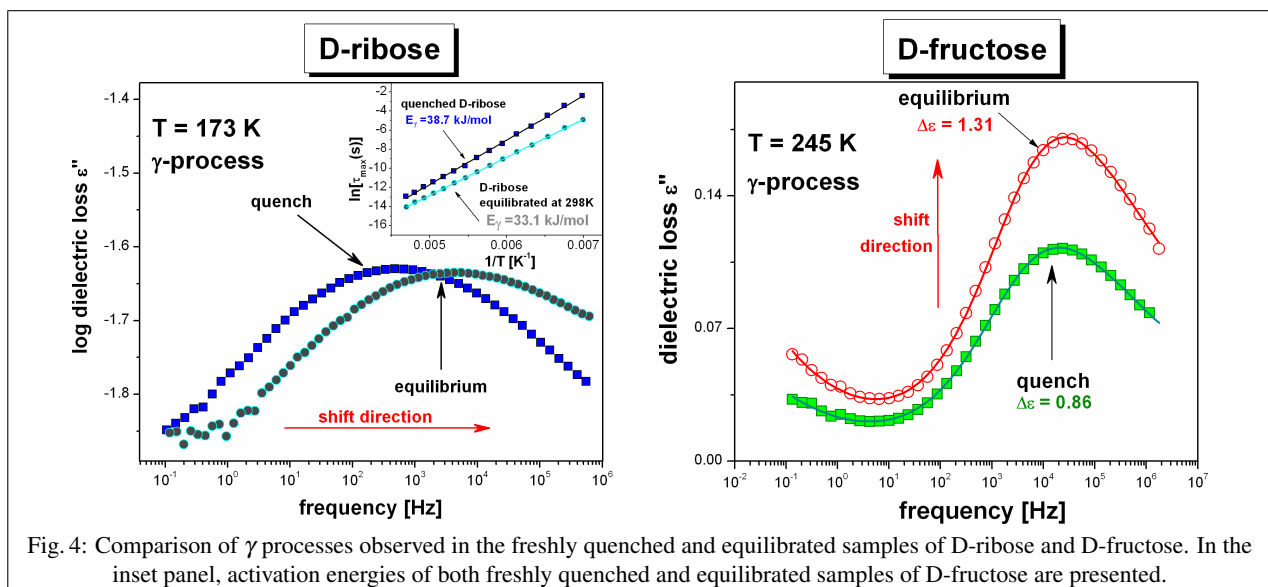


Fig. 4: Comparison of γ processes observed in the freshly quenched and equilibrated samples of D-ribose and D-fructose. In the inset panel, activation energies of both freshly quenched and equilibrated samples of D-fructose are presented.

The first measurement has been performed instantly, the second one after two days of equilibrating the sample at a temperature above the glass transition temperature.

In Fig. 4, one can see that the amplitude of the dielectric loss ϵ'' attributed to the γ process of D-fructose increases by about 50% during mutarotation, whereas the relaxation time does not change at all. A quite different effect is observed in the case of D-ribose – while the dielectric strength is almost the same, the relaxation time is shifted about one decade towards higher frequencies. Moreover, the activation energy has diminished from 38 to 33 kJ/mol [2,3]. The last but not least is the application of dielectric spectroscopy to the analysis of tautomerization phenomenon under compression. It is well known that the BDS technique can be easily extended to the study at elevated pressure. Thus, the analysis of tautomerism phenomenon under compression is also possible. The exemplary pressure effect on the mutarotation rate constant has been already presented in our previous work [3].

References

- [1] M. B. Smith and J. March, *Advanced Organic Chemistry*, 5th ed. Wiley Interscience, New York, 2001, pp. 1218–1223.
- [2] P. Włodarczyk, K. Kaminski, S. Haracz, M. Dulski, M. Paluch, J. Ziolo, M. Wyględowska-Kania, *J. Chem. Phys.* 132, 1 (2010).
- [3] P. P. Włodarczyk, K. Kaminski, M. Paluch, J. Ziolo, *J. Phys. Chem. B*, 113, 4379–4383 (2009).
- [4] Z. Wojnarowska, K. Grzybowska, K. Adrjanowicz, K. Kaminski, M. Paluch, L. Hawelek, R. Wrzalik, M. Dulski, W. Sawicki, J. Mazgalski, A. Tukalska T. Bieg, *Mol. Pharmaceutics*, (2010), 7 (5), pp 1692–1707.
- [5] Z. Wojnarowska, P. Włodarczyk, K. Kaminski, K. Grzybowska, L. Hawelek, M. Paluch *J. Chem. Phys.* 133, 8 (2010) doi:10.1063/1.3475688.
- [6] P. Włodarczyk, K. Kaminski, M. Dulski, S. Haracz, M.

Paluch, J. Ziolo, *J. Non-Cryst. Solids*, Volume 356, 738-742 (2010).

Z. Wojnarowska, P. Włodarczyk, and M. Paluch¹

Institute of Physics, University of Silesia, ul. Uniwersytecka 4, 40-007 Katowice, Poland

¹marian.paluch@us.edu.pl

Gennady F. Novikov
and Nikolay A. Radychev

Broadband Photodielectric Spectroscopy

There are a large number of materials known which demonstrate a variation of the complex permittivity ϵ^* by light excitation or ionizing radiation. Variations can be both reversible and irreversible. Irreversible modifications, e.g., are observed during photopolymerization, photocrosslinking and other photochemical reactions. In the case of reversible effects, the variation of the imaginary part of the permittivity, $\Delta\epsilon''$, is usually called *photoconductivity*, while the variation in its real part, $\Delta\epsilon'$, is called the *photodielectric effect*. Quite a lot of materials show the photodielectric effect, e.g., organic and inorganic compounds, crystalline and amorphous matters, materials based on short molecular chains and long oligomeric or polymeric molecules. In the above listed group of materials, the semiconductors possess maximal "sensitivity" to light influence. Application of ionizing radiation allows for the investigation of a medium with high ionization potential including heterogeneous, opaque and scattering media. In this case, the variation in $\Delta\epsilon'$ is called the *radiative photodielectric effect*.

Despite the fact that the photodielectric effect was discovered almost half a century ago, its nature is still poorly understood. Important information about the photodielectric effect and, therefore, the properties of the investigated matter can be obtained by broadband dielectric spectroscopy (BDS). In this communication, we present broadband photodielectric spectroscopy (BPDS) on polycrystalline thin CdS films as a showcase for the study of the generation and loss processes of photogenerated carriers.

Experimental details

CdS thin films (5 μm ...10 μm) were obtained by spraying an aqueous solution of chloride thiourea coordination compounds (TCC) of cadmium on a substrate heated to 500 °C [1]. TCC decomposition with formation of a sulfide film occurred. A broadband dielectric spectrometer BDS - *Concept Eight* by Novocontrol was upgraded with an illumination system with calibrated light. The samples were illuminated with monochromatic light using a xenon lamp DKSSh-1000 with a monochromator. The samples were illuminated in a range of wavelengths $\lambda = 350 \dots 2500 \text{ nm}$. During the measurements the monochromator apertures were checked so that light intensities with various wavelengths would not differ by more than by a factor of two. The average intensity I_0 was about $10^{15} \text{ photons cm}^{-2}\text{s}^{-1}$. Finally, the results of the measurements were normalized with respect to the light intensity.

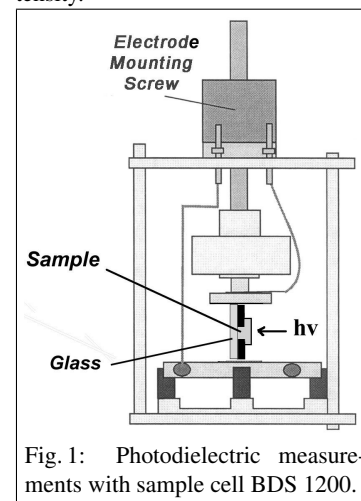


Fig. 1: Photodielectric measurements with sample cell BDS 1200.

Measurements were carried out in a planar type cell with vacuum evaporated aluminum electrodes. The typical electrode gap was 0.2 mm. Temperature control for the samples with evaporated electrodes was provided using a specially made cryostat equipped with an illumination window. Fig. 1 shows as an example the use of the sample cell BDS 1200. Measurements were carried out in the frequency range $10^{-3} \dots 10^5 \text{ Hz}$, and the temperature range from -100 °C to +100 °C.

The observed $\epsilon^*(\omega)$ spectra (where $\omega = 2\pi f$ is the frequency of the electric field) were fitted by the sum of two Havriliak-Negami (H-N)

functions with DC conductivity using Novocontrol Technologies WinFIT 2.9:

$$\begin{aligned} \epsilon^* &= \epsilon' - i\epsilon'' \\ &= \sum_{j=1}^2 \left[\frac{\Delta\epsilon'_j}{(1 + (i\omega\tau_j)^{\alpha_j})^{\beta_j}} + \epsilon_{\infty j} \right] \\ &\quad - i \left(\frac{\sigma_0}{\epsilon_0\omega} \right)^N \end{aligned} \quad (1)$$

which made it possible to determine the distribution of dielectric relaxation times, $G(\tau)$.

Results

In Fig. 2 (curve 1) the dependence of the loss tangent on electric field frequency, $\text{tg}\delta(f)$, is shown for measurements performed in the dark. One can see that the dependence $\text{tg}\delta(f)$ monotonically decreases toward high frequencies in the presented frequency range. Only a weak maximum (not shown in Fig. 2) is observed at a frequency of ca. 2 Hz, which corresponds to the relaxation time of approx $6.3 \cdot 10^{-2}$ s. During constant illumination, we find a maximum in the $\text{tg}\delta(f)$ spectra; its position depends on the wavelength of light (Fig.2, curves 2 and 3).

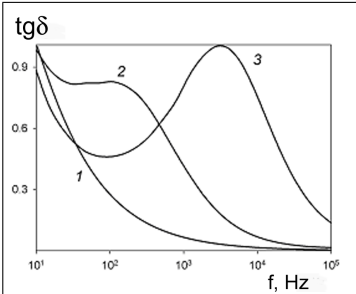


Fig. 2: Dependence of the loss tangent on electric field frequency. 1: dark; 2: $\lambda = 840$ nm; 3: $\lambda = 600$ nm; $\theta = 20^\circ\text{C}$.

As shown in in Fig. 3 for $\lambda = 400$ nm, the maximum values of $\text{tg}\delta(f)$, within experimental error, do not depend on the light intensity. Dependences $\epsilon''(f)$ and $\epsilon'(f)$ under lighting in the wavelength range from 350 nm to 840 nm show a complex form. As an example, the separation of the experimental $\epsilon''(f)$ (curve 1, taken at $\lambda = 430$ nm) into the DC conductivity (curve 2) and dipole relaxation parts (curve 3) is shown in Fig. 4, with two characteristic relaxation times (inset, curve 3' and 3'').

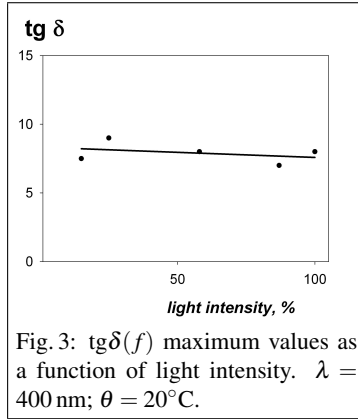


Fig. 3: $\text{tg}\delta(f)$ maximum values as a function of light intensity. $\lambda = 400$ nm; $\theta = 20^\circ\text{C}$.

A decrease in the photon energy makes one of the $\epsilon''(f)$ maxima vanish. As a consequence, the $\epsilon''(f)$ spectra in the wavelength range from 880 nm to 2500 nm were fitted by only one H-N function.

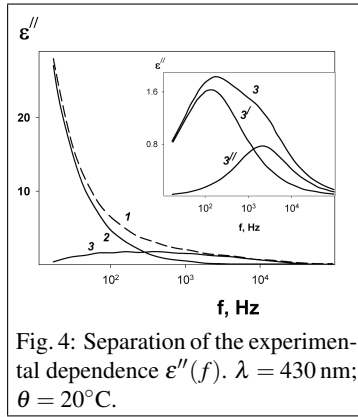


Fig. 4: Separation of the experimental dependence $\epsilon''(f)$. $\lambda = 430$ nm; $\theta = 20^\circ\text{C}$.

Relaxation time distributions, $G(\tau)$, are shown for different photon energies E in Fig. 5. With photon energy decreasing from 3.5 eV to 1.5 eV, the maximum is shifted towards higher relaxation times. At $E < 1.5$ eV, one maximum of $G(\tau)$ disappears and the other shifts to the dark value, which corresponds to the behavior of the peak in the $\epsilon''(f)$ spectra discussed above.

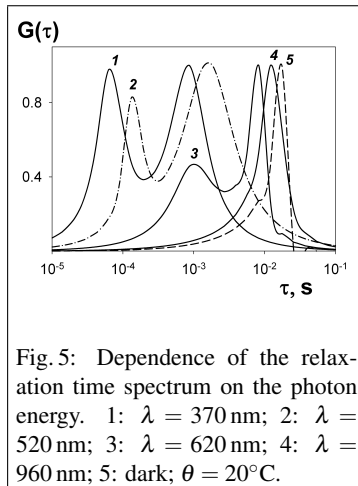


Fig. 5: Dependence of the relaxation time spectrum on the photon energy. 1: $\lambda = 370$ nm; 2: $\lambda = 520$ nm; 3: $\lambda = 620$ nm; 4: $\lambda = 960$ nm; 5: dark; $\theta = 20^\circ\text{C}$.

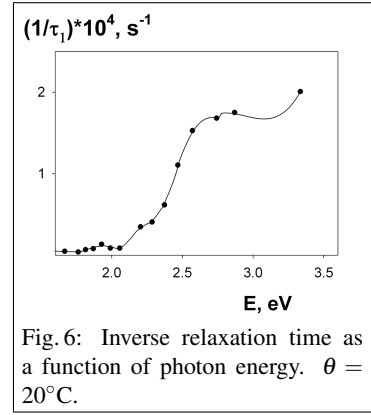


Fig. 6: Inverse relaxation time as a function of photon energy. $\theta = 20^\circ\text{C}$.

The inverse relaxation time τ_1^{-1} as a function of photon energy for 20°C is represented in Fig. 6. The dependence of τ_1^{-1} on the light intensity, determined at $\lambda = 400$ nm turns out to be linear, cf. Fig. 7.

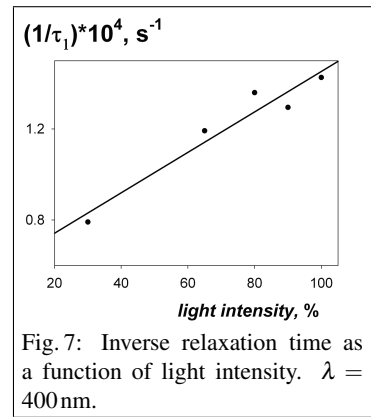


Fig. 7: Inverse relaxation time as a function of light intensity. $\lambda = 400$ nm.

When the temperature drops from 20°C to -50°C , there are pronounced changes in the distribution of relaxation times.

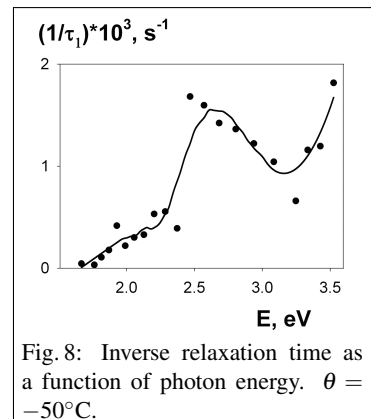


Fig. 8: Inverse relaxation time as a function of photon energy. $\theta = -50^\circ\text{C}$.

The inverse relaxation time $\tau_{1,2}^{-1}$, plotted as a function of photon energy (Fig. 8.) demonstrate a wide maximum along the stable main curve arising in the energy range $E = 2.5 \dots 3$ eV. When the temperature is dropped further to $\theta = -100^\circ\text{C}$, the maximum changes to a narrow peak with $E_{\text{max}} = 2.5$ eV (Fig. 9).

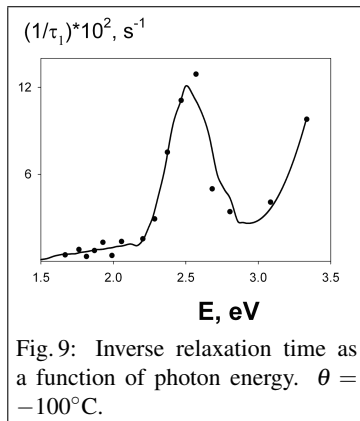


Fig. 9: Inverse relaxation time as a function of photon energy. $\theta = -100^\circ\text{C}$.

Discussion

The interpretation of the the presented experimental data is difficult in the limited scope of this short communication. However it is important to note that dielectric parameters of the samples change by impact of light with energy $h\nu \gg k_B T$ (k_B being Boltzmann's constant). It is therefore natural to infer that this change is associated with charge carrier generation. This assumption is further corroborated by the observed linear dependence of $\tau_{1,2}^{-1}$ on the light intensity (Fig. 7). In view of the observed independence of $\text{tg}\delta$ on light intensity, it is also possible to assume that one and the same particle is responsible for changes in both the conductivity and dielectric permittivity of the samples. In our case it is the electrons. Such an assumption does not contradict the obtained data of photoconductivity of CdS. As demonstrated in Fig. 10, the spectral distribution curve for CdS (1) from [2] coincides with the experimental photocurrent data (2 and 3). Curve 2 shows the DC conductivity, curve 3 the experimental current values at a frequency of 10 Hz, respectively. At the same time, the appearance of two peaks in the relaxation time distribution, one of which disappears with decreasing photon energy below 1.5 eV, indicates their different nature. The bandgap E_g of CdS is about 2.4 eV. Therefore the left edge of the narrow peak on $\tau_1^{-1}(f)$ with $\theta = -100^\circ\text{C}$ (Fig. 9) belongs to the energy region close to the bottom edge of CdS bandgap. This gives rise to the assumption that formation of the narrow peaks (Fig. 8, Fig. 9) may be associated with creation and thermal dissociation of excitons. We may, e.g., envisage an exciton corresponding to an interstitial

atom of sulfur ($\lambda = 488.5$ nm) or an exciton corresponding to an interstitial atom of cadmium and lattice vacancy of sulfur ($\lambda = 487$ nm).

It is an important result that electrons and holes are formed by light with energy $E \geq E_g$, either due to the thermal dissociation of the exciton or as a result of the interband transition. The life times of the free formed charges, which are characterized by the kinetic rules [3] are quite small. However, trapping (by, e.g. crystalline grains, dislocations, defects) prolongates the charge carrier lifetimes significantly. In this case, the lifetimes should be determined by the depth of the traps. Relaxation times for dark measurements are described by the Arrhenius equation

$$\tau^{-1} = \tau_0^{-1} \exp \left\{ -\frac{E_a}{k_B T} \right\} \quad (2)$$

where E_a , k_B , and τ_0^{-1} are the thermal trap depth, Boltzmann's constant, and the pre-exponential factor, respectively. It is natural to assume a similar equation for processes under light excitation.

$$\tau^{-1} = \beta s I, \quad (3)$$

with β , s , and I representing the quantum yield, the absorption cross section, and the light intensity, respectively.

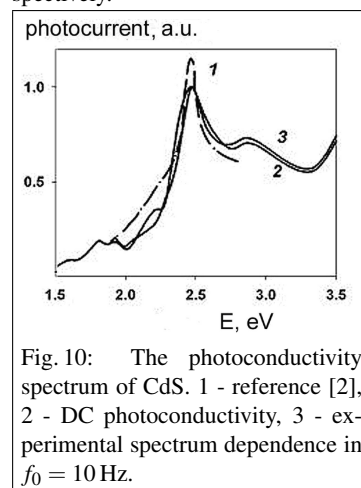


Fig. 10: The photoconductivity spectrum of CdS. 1 - reference [2], 2 - DC photoconductivity, 3 - experimental spectrum dependence in $f_0 = 10$ Hz.

The spectral dependence of the relaxation time is determined by the product βs (the cross section of the ionization). It is clear that the data in Fig. 10 correlates well with Figs. 7, 8 and 9. The electron escape time under illumination with intensity 10^{15} photons $\text{cm}^{-2} \text{s}^{-1}$ and trap cross section $s = 10^{-17} \dots 10^{-18} \text{cm}^2$ is about $10^{-2} \dots 10^{-3} \text{s}$. This is well in line

with the times observed in our experiment. The impurity centers in the semiconductor bandgap must be involved in charge formation with energy $E < E_g$ [4]. In this case, electron-hole pairs are not created and only one kind of the carrier is responsible for DC conductivity. In conclusion we should like to emphasize that the presented example for the application of Broadband Photodielectric Spectroscopy to studying the photodielectric effect in CdS is only a limited illustration of the large number of opportunities that this method offers for the research of photosensitive systems. This method introduces two additional independent variables to the study of these systems: the incident light quantum energy and intensity. Moreover, the method may also well be expanded to the investigation of objects in the sub-nanometer range.

References

- [1] Meteleva Yu.V., Naumov A.V., Sermakasheva N.L., Semenov V.N., Novikov G.F., *Rus. J. Phys. Chem. B.* **20**, 39-45 (2001).
- [2] R.H. Bube, *Photoconductivity of Solids*, Wiley, New York, 1960, p.127.
- [3] G.F. Novikov, N.A. Radychev, *Russ. Chem. Bull.* **5** (2007) 890-894.
- [4] N.A. Radychev, G.F. Novikov, I.A. Chernov, and Yu.V. Meteleva, *Russ. J. Phys. Chem. A. V.* **79** (2005) 1867-1869.

Gennady F. Novikov¹
and Nikolay A. Radychev

Institute of Problems of Chemical Physics
Russian Academy of Sciences
Chernogolovka, Moscow region,
Russia. 142432
¹ngf@icp.ac.ru

D. Wilmer

New Developments of Novocontrol Technologies

Novocontrol Technologies has recently introduced new versions of its temperature control systems for high temperatures, viz., **Novotherm-HT**, with maximum temperatures of 1200°C , 1400°C , and 1600°C , respectively.

These systems are intended for electrical characterisations of high-temperature materials (e.g., oxide ceramics, fuel-cell and sensor components etc.) and consist of a furnace, a temperature controller and a dedicated high-temperature cell made of alumina and platinum parts, mounted into a 19" lab tray. Besides front panel operation, they are prepared for remote control from a computer and for combined operation with an impedance analyzer. A highly recommended solution includes a Novocontrol Alpha-A frequency response analyzer mainframe with DC bias option and ZG4 test interface, or an Alpha-A with one of our POT/GAL test interfaces. Further addition of a WinDETA software with temperature control option yields a fully automatic set-up for electrical measurements of materials as a function of frequency and temperature (and others like AC or DC voltages or currents), with particular emphasis to high temperatures up to 1600 °C.

The Novotherm-HT now includes an original temperature controller manufactured by Novocontrol Technologies, offering quick and highly stable control up to the highest temperatures.



New Novotherm-HT controller: front panel.

The controller works in cascading mode and comes with a GPIB interface; it receives input from two Pt/PtRh thermocouples (one to monitor the furnace, the other to read the sample temperature). In contrast

to less elaborate solutions, the controller regulates the sample temperature, not just the furnace temperature, allowing the user to set and get the temperature at the sample that is really desired. The new controller uses a highly successful method to suppress thermocouple reading instabilities at very high temperatures. Up to 1300 °C, measurements can be performed using an additional grounded metal shield which reduces electrical noise in the impedance measurements (particularly useful for high-impedance samples). As the use of the extra shield changes the temperature control loop characteristics, the Novotherm-HT controller offers two control modes for operation with or without additional shield.

The controller comes with five automatically selected sets of PID parameters which allow perfect adaptation of the control characteristics to the given temperature. The resulting performance over the entire temperature range is exemplified in the figure below (left panel).

Novocool Cryosystem

Another improvement concerns the **Novocool Cryosystem** which covers temperatures between -100 °C and +250 °C and is fully compatible with the Novocontrol sample cells BDS 1200 and ZGS (Alpha-A active sample cell). Major improvements are the *active adaptation of the nitrogen pressure* and thus regulation of the coolant flow, leading to a *decreased nitrogen consumption with improved temperature stability*. An example showing the temperature control performance of the new Novocool Cryosystem is given in the figure below (right panel).

WinCHEM 2.0

Novocontrol recently released **WinCHEM 2.0**, a new version of our electrochemical software to support the Alpha-A Potentiostat/Galvanostat (POT/GAL) test interfaces for current/voltage measurements in the time domain. WinCHEM 2.0 now provides an extended input scheme, allowing the user to enter additional arbitrary waveforms (of voltage or current). These are easily provided as plain text files. As a consequence, the Alpha-A POT/GAL test interface, when operated with WinCHEM 2.0, can be used as a sophisticated function generator for arbitrary waveforms.

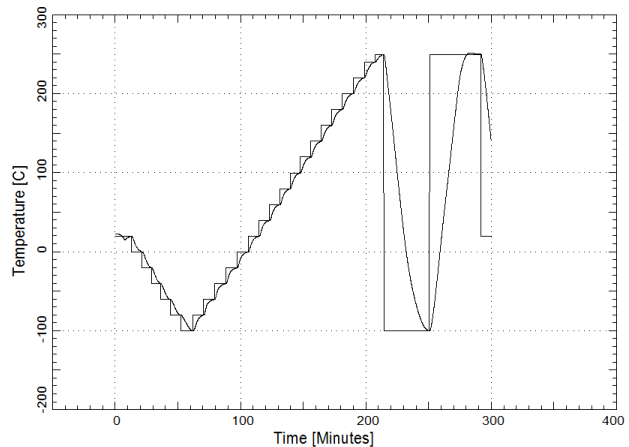
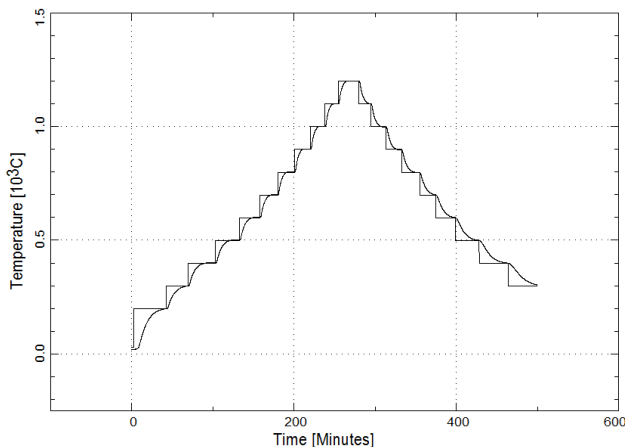
Windows 7 Compatibility

All our software packages, i.e., **WinDETA/WinIMP**, **WinCHEM**, **WinTSC**, and **WinFIT** now fully support the most recent versions of Microsoft Windows, i.e., Windows 2000, XP, Vista, and Windows 7. This was achieved with the help of completely new setup routines for all packages and a complete re-write of the drivers for our GPIB interface, BDS 1500.

Training Course

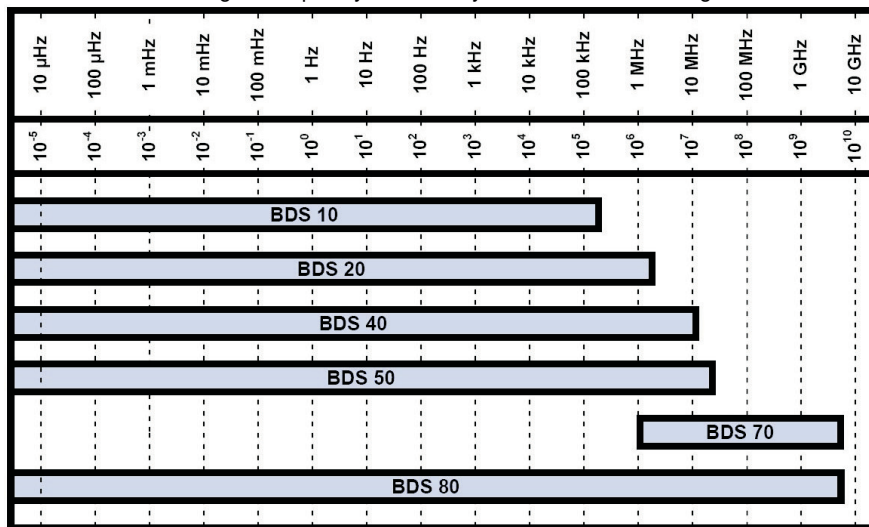
Novocontrol Technologies announces its third **Training Course on Broadband Dielectric and Impedance Spectroscopy** to take place September 26-28, 2011, at the University of Marburg, Germany under the guidance of Profs. F. Kremer and B. Roling. **Registration deadline is September 2, 2011.** For further details, see our web pages, under "Training Courses & Seminars".

D. Wilmer
Novocontrol Technologies



Novotherm-HT 1200 (left) and Novocool Cryosystem (right) temperature control performance. Lines symbolize setpoint (staircase) and process values, respectively.

OVERVIEW

BROADBAND DIELECTRIC AND IMPEDANCE SPECTROSCOPY
covering 16 frequency decades by Novocontrol Technologies

Factory and Head Office

Germany

Novocontrol Technologies GmbH & Co. KG
Obererbacher Straße 9
56414 Hundsangen/GERMANY
Contact: Dr. Dirk Wilmer

Phone: +49 6435 9623-0
Fax: +49 6435 9623-33
Mail: novo@novocontrol.de
Web: www.novocontrol.de

Agents

USA/Canada

Novocontrol America Inc.
Wake Forest, NC 27587 / USA
Toll free: +1 866 554 9904
Phone: +1 919 554 9904
Fax: +1 919 573 0373
Mail: novocontrolusa@earthlink.net
Contact: Mr. Joachim Vinson, PhD

Japan

Morimura Bros. Inc.
Minato-Ku, Tokyo 105 / Japan
Phone: +81 3-3502-6440
Fax: +81 3-3502-6437
Mail: s-hasegawa@morimura.co.jp
Contact: Mr. Shintaro Hasegawa

People's Republic of China

GermanTech Co. Ltd
Beijing, 100083 / China
Phone: +86 10 82867920/21/22
Fax: +86 10 82867919
Mail: contact@germantech.com.cn
Contact: Mrs. Xiaoyu Sun

South Korea

HI Corporation
Anyang-shi, Kyungki-Do, Korea
Phone: +82 31 479 6250
Fax: +82 31 479 6255
Mail: hicorpkim@chol.com
Contact: Mr. Jason Kim

India

A-Tech Systems
Mumbai 400 080, India
Phone: +91 22 2294 3222 and 2164 0515
Fax: +91 22 2164 0525
Mobile: +91 22 9322 255 717
Email: arvind.atech@gmail.com
contact: Mr. Arvind Panchal

India

Sinsil International HO
Mumbai 400 607
Mobile: +91 9833011933
Mobile: +91 9870225777
Mail: sinsilmumbai@gmail.com
Contact: Dr. K. Ramesh

Turkey

TEKNO TIP Analitik Sistemler Ltd. Sti.
06570 Cankaya / Ankara, TURKIYE
Phone: +90 312 236 4208
Fax: +90 312 236 4218
Email: eyenihayat@teknopip.com.tr
contact: Mr. Erman Yenihayat

Greece

Vector Technologies Ltd.
15234 Halandri, Athens
Phone: +30 210 685 8008
Fax: +30 210 685 8118
Mail: info@vectortechologies.gr
Contact: Mr. Vouvous

Editor: Dirk Wilmer. Abstracts and papers are always welcome. Please send your manuscript to the editor.